Supporting Information

Spectroscopy and DFT calculations of a flavo-diiron enzyme implicate new diiron site structures

Andrew C. Weitz, Nitai Giri, Jonathan D. Caranto, Donald M. Kurtz, Jr., Emile L. Bominaar, and Michael P. Hendrich

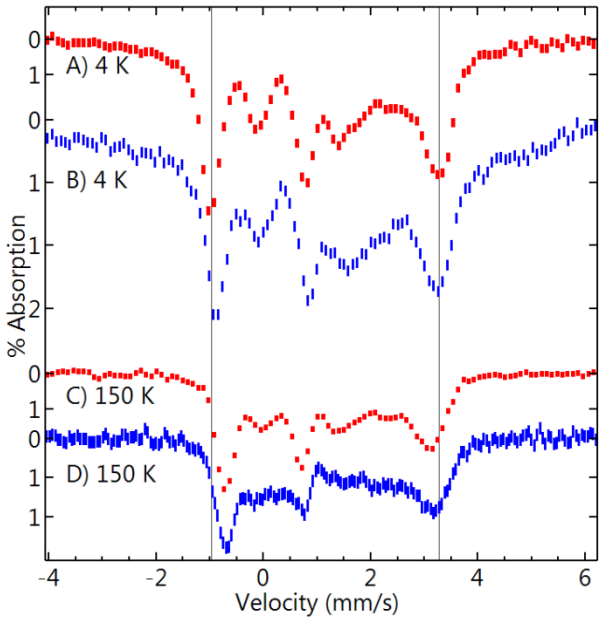

Figure S1. Mössbauer spectra of FDP_{red} (A, C) deflavo-FDP_{red} (B, D) for a magnetic field of 7 T recorded at the temperatures listed.

Table S1. Comparison of DFT results for J, δ, and ΔE_Q in diferric state of FDP for various bridging arrangements with experiment.

	Bridge(s)[a]	J[b] cm^{-1}	Fe_P[c]			Fe_D[c]		
			δ mm/s	ΔE_Q mm/s	η	δ mm/s	ΔE_Q mm/s	η
1$_3$	O^{2-}	+208	0.41	–1.98	0.35	0.49	–1.50	0.23
2$_3$	$OH^-\cdots OCO^-$	+45.3	0.39	+1.01	0.60	0.45	–0.55	0.26
2$_3^{NW}$	$OH^-\cdots OCO^-$	+46.9	0.42	+0.97	0.14	0.38	+1.17	0.67
3$_3$	$HO^-\cdots HOCO$	+11.4	0.40	+1.18	0.27	0.45	–1.09	0.90
4$_3$	$HOH\cdots OCO^-$ [d]	+1.2	0.43	+1.20	0.41	0.71[e]	+1.10	0.25
5$_3$	$OH^-\cdots OHCO$	+32.7	0.41	+0.73	0.75	0.44	+1.10	0.19
6$_3$	OH^-	+30.0	0.39	+0.92	0.54	0.45	+0.36	0.62
7$_3$	$OH^-\cdots OCO^-$; OH^-	+19.2	0.50	+0.64	0.73	0.48	–0.78	0.87
7$_3^{NHB}$	OH^-; OH^-	+19.4	0.49	+0.68	0.38	0.53	–0.51	0.22
exp		+20	0.48	+1.04	0.6	0.43	0.94	1

[a] The carboxylate bridge, present in all structures, has not been listed, ··· represents H-bonding. [b] $J = (E_F - E_{BS})/12.5$, E_F and E_{BS} are the B3LYP/6-311G system energies obtained for optimized F and BS geometries, respectively. [c] Parameters calculated for the BS state; the values calculated for the F state are only marginally different. [d] One H-OH distance has been fixed to typical H-O distance in water to prevent transfer of the proton to the carboxylate (resulting in **4**$_3$). [e] This value is slightly higher due to partial oxidation of one the tyrosines. This charge shift has been prevented from happening in **5**$_3$ by stabilizing the tyrosines by hydrogen bonds donated by auxiliary waters.

Table S2. Comparison of DFT results for J, δ, and ΔE_Q in diferrous state of FDP for various bridging arrangements with experiment.

	Bridge	J cm^{-1}	Fe_P			Fe_D		
			δ mm/s	ΔE_Q mm/s	η	δ mm/s	ΔE_Q mm/s	η
$\mathbf{1}_2$	O^{2-}	+230	1.01	+1.26	0.44	0.83	–0.43	0.44
$\mathbf{2}_2$	$OH^-\cdots OCO^-$	+37.9	1.11	+1.80	0.16	1.24	+2.61	0.01
$\mathbf{2}_2^{NW}$	$OH^-\cdots OCO^-$	+48.1	1.13	+2.08	0.20	1.13	+2.32	0.60
$\mathbf{3}_2$	$HO^-\cdots HOCO$ [a]	+10.1	1.14	+2.81	0.51	1.24	+3.39	0.12
$\mathbf{3}_2^{NW}$	$HO^-\cdots HOCO$	+9.7	1.12	+2.54	0.41	1.12	+2.85	0.46
$\mathbf{4}_2$	$HOH\cdots OCO^-$	+2.9	1.15	+2.62	0.44	1.24	+3.02	0.18
$\mathbf{5}_2$	$OH^-\cdots OHCO$	+11.8 +8.9	1.13 1.15	+2.12 +2.78	0.25 0.49	1.22 1.24	+2.91 +3.27	0.59 0.13
$\mathbf{5}_2^{NW}$	$OH^-\cdots OHCO$ [b] [c] [d]	+39.1 +31.7 +35.6	1.11 1.14 1.04	+2.38 +2.71 +2.07	0.25 0.11 0.78	1.08 1.15 1.10	+1.99 +2.10 +2.15	0.16 0.10 0.09
$\mathbf{6}_2$	OH^-	+23.8	1.12	+1.88	0.22	1.25	+3.07	0.34
$\mathbf{6}_2^{NW}$	OH^-	+35.2	1.13	+2.14	0.14	1.16	+2.25	0.46
$\mathbf{7}_2$	$OH^-\cdots OCO^-$ [f] OH^-	–7.4	1.27	+2.56	0.27	1.27	+2.85	0.15
exp		+32(5)	1.15	2.42	–	1.15	2.42	–

[a] H-OCO bond distance fixed in optimization. [b] Carboxylate at Fe_D is hydrogen bonded to Tyr. [c] Carboxylate at FeD is hydrogen bonded to auxiliary water. [d] Both terminal carboxylates are protonated.

Table S3. J and metrics of models for FDP_{ox} and FDP_{red} from DFT

	J (cm^{-1})	Fe···Fe (Å)	Fe-O_H-Fe (°)	Fe_P-O_H (Å)	Fe_D-O_H (Å)	O_H···O_{carbox} (Å)
$\mathbf{2}_3$	45.3	3.610	135.3	1.926	1.978	2.606
$\mathbf{2}_3^{NW}$	46.9	3.683	141.3	1.964	1.940	2.618
$\mathbf{2}_2$	37.9	3.524	128.0	1.915	2.005	2.676
$\mathbf{2}_2^{NW}$	48.1	3.587	134.8	1.931	1.954	2.658
$\mathbf{3}_3$	11.4	3.710	124.5	2.098	2.095	2.636
$\mathbf{3}_2$	10.1	3.571	114.9	2.094	2.143	2.513
$\mathbf{3}_2^{NW}$	9.7	3.677	121.6	2.130	2.082	2.529
$\mathbf{4}_3$	1.2	3.854	121.1	2.159	2.267	2.445
$\mathbf{4}_2$	2.9	3.684	112.6	2.174	2.253	2.480
$\mathbf{5}_3$	32.7	3.668	133.3	2.000	1.996	2.949
$\mathbf{5}_2$	11.8 8.9	3.588 3.605	124.2 113.9	1.976 2.128	2.084 2.173	3.953 3.953
$\mathbf{5}_2^{NW}$ [a] [b] [c]	39.1 31.7 35.6	3.573 3.569 3.544	133.3 128.7 130.4	1.955 1.994 1.929	1.938 1.965 1.974	2.682 3.423 2.672
$\mathbf{6}_3$	30.0	3.682	135.5	1.947	2.031	4.321
$\mathbf{6}_2$	23.8	3.537	124.6	1.925	2.070	4.303
$\mathbf{6}_2^{NW}$	35.2	3.592	121.6	1.953	1.985	3.374
$\mathbf{7}_3$	19.2	3.139	98.3 104.8	2.116 1.976	2.033 1.986	2.666
$\mathbf{7}_3^{NHB}$	19.4	3.188	102.4 105.9	2.067 1.996	2.024 1.998	3.924
$\mathbf{7}_2$	–7.4	3.051	93.7 94.8	2.160 2.321	2.019 2.121	2.762

[a] Carboxylate H-bond to Tyr. [b] Carboxylate H-bond to water. [c] Doubly protonated.

Table S4. J predictions for hydroxo and alkoxo bridged binuclear Fe^{3+} complexes.

#GL[a]	CCSD[b]	Bridges [c]	J_{exp}[d] cm^{-1}	P_{GL} (XR) Å	J_{GL} (XR)[e] cm^{-1}	P_{GL} (DFT)[f] Å	J_{GL} (DFT)[g] cm^{-1}	J (DFT) cm^{-1}
1	PICAFE	OH, OH	14.6	1.964	27.7	1.980	31.4	26.8
3	FESLED11	OR, OR	15.0	2.080	6.4	2.089	7.9	15.4
6	CAHJEA	OH, OH	20.8	2.021	13.5	2.034	16.0	16.2
7	CUPXED	OR, OR	22.0	1.982	22.1	1.991	27.3	25.2
9	HXAPFE	OH, OH	23.4	1.962	28.4	1.981	31.2	27.6
10	DEWPIE10	OH, OR	24.0	1.960	29.2	1.999	24.7	28.3
11	CUPXAM	OR, OR	30.8	1.991	19.7	2.001	25.0	28.5
13	COCJIN	OH, CB, CB	34.0	1.956	30.7	2.019	19.2	30.5
15	JEZVUF	OR, OR	41.0	2.000	17.6	2.019	19.2	40.4
[h]	CEPBEF	OH	42, 43	1.997	18.2	2.016	19.9	46.8

[a] Labels in Table 1 of Gorun and Lippard, *Inorg. Chem*. **1991**, *30*, 1625-1630. [b] Label from Cambridge Crystallographic Structure Database of structure used for obtaining exchange path length P_{GL} (XR). [c] OR = alkoxo, CB = carboxylate. [d] **1** *J. Am Chem. Soc.* **1976**, *98*, 1425; **3** *J. Am. Chem. Soc*. **1968**, *90*, 6347 and *J. Chem. Soc*. A **1967**, 1900; **6** *Inorg. Chem*. **1983**, *22*, 1719; **7** *Inorg. Chem*. **1984**, *23*, 3398; **9** *J. Am. Chem. Soc*. **1978**, *100*, 2053; **10** *J. Am. Chem. Soc*. **1985**, *107*, 6728, *ibid.* **1987**, *109*, 7993; **11** *Inorg. Chem*. **1984**, *23*, 3398; **13** *J. Am. Chem. Soc*. **1984**, *106*, 4632; **15** *Inorg. Chem*. **1990**, *29*, 4293. [e] J (in $J\boldsymbol{S}_1\cdot\boldsymbol{S}_2$) obtained from GL relation between J and GL exchange path length P_{GL} from X-ray structure, $J_{GL} = 17.526 \times 10^{11} \exp[-12.663 \times P_{GL}]$. [f] GL exchange path length obtained from DFT optimized structure using B3LYP/6-311G. [g] J (in $J\boldsymbol{S}_1\cdot\boldsymbol{S}_2$) obtained from scaled GL relation between J and GL exchange path length P_{GL} from DFT structure. As the DFT distances are systematically longer than the XR distances, the J values predicted with the GL relation have been scaled by the factor 1/0.72. [h] *Inorg. Chem*. **2006**, *45*, 6922. Experimental values from magnetic susceptibility and Mössbauer, respectively.

Table S5. Bridges, metric data, and J values from experiment and DFT for diferric model complexes.

CCSD[b]	Bridges [a]	Fe···Fe Å		Fe-O-Fe °		J cm^{-1}	
		XR	DFT	XR	DFT	Exp	DFT
PICAFE	OH, OH	3.089	3.125	103.6	104.2	14.6	26.8
FESLED11	OR, OR	3.289	3.284	104.6	103.6	15.0	15.4
CAHJEA	OH, OH	3.155	3.199	102.8	103.7	20.8	16.2
CUPXED	OR, OR	3.117	3.126	103.6	103.5	22.0	25.2
HXAPFE	OH, OH	3.119	3.132	105.3	104.5	23.4	27.6
DEWPIE10	OH, OR	3.137	3.152	106.3, 102.5	104.0; 102.5	24.0	28.3
CUPXAM	OR, OR	3.144	3.128	104.3	102.8	30.8	28.5
COCJIN	OH, CB, CB	3.438	3.444	123.0	127.8	34.0	30.5
JEZVUF	OR, OR	3.213	3.259	107.4	107.6	41.0	40.4
CEPBEF	OH	3.929	3.906	159.5	151.4	42, 43	46.8

[a] OR = alkoxo, CB = carboxylate. [b] Label from Cambridge Crystallographic Structure Database.

Table S6. δ and ΔE_Q calibration for high-spin Fe^{2+} and Fe^{3+} complexes and comparison with experiment.

CCSD	Group[a]	State[b]	ρ(0) – 11614	δ_{DFT}[c]	δ_{Exp}[d]	$\Delta E_{Q\ DFT}$[e]	η_{DFT}	$\Delta E_{Q\ Exp}$[f]
Fe^{2+}								
TPYFEC	C_1	–	0.371	1.09	1.16	+3.53	0.00	+3.14
DEBWEM	C_{2v}	–	0.262	1.14	1.00[g]	–3.10	0.00	–3.27
DIBWUG10	C_1	F	0.087	1.22	1.16	+2.70	0.83	+2.83
GATFUC	C_{2h}	F	0.180	1.18	1.24	+2.89	0.56	+2.72
KASFUF	C_{2h}	F	0.268	1.14	1.11	–2.05	0.11	2.24
Fe^{3+}								
CAVDOS05	C_1	–	1.893	0.43	0.54	–0.36	0.61	0.24
DALLIL	C_1	–	1.395	0.65	0.56	–0.02	0.17	0.04
FACTEI	D_{3d}	F	2.054	0.37	0.36	–1.62	0.00	1.24
TEMKUR	C_1	F	1.572	0.57	0.56	–1.37	0.87	0.90
VABMUG	C_2	F	1.777	0.49	0.41	–1.54	0.50	1.80
YOHMOX	C_1	BS	1.876	0.44	0.46	+1.30	0.93	1.41
COCJIN	C_1	F	1.834	0.46	0.50	–0.36	0.12	0.25
YOCKAC	C_{2h}	F	1.765	0.49	0.50	–1.79	0.84	1.93
DIBXAN10	C_{2h}	F	1.845	0.46	0.47	–1.54	0.20	1.50
CAHJEA	C_i	BS	1.653	0.54	0.49	–0.69	0.89	0.56

[a] Symmetry group of model used for DFT calculation. [b] The metal centers listed in the table are high spin. Mononuclear complexes have been indicated with a "–" and binuclear complexes are labeled "F" of "BS", depending on whether the ferromagnetic state or the broken symmetry state was used for the calculation of the hyperfine parameters. [c] $\delta_{DFT} = 1.25383 - 0.432609\ (\rho(0) - 11614\ a_0^{-3})$. [d] ^{57}Fe isomer shift at 4.2 K, Exp refers to experimental. [e] $\Delta E_Q = (1 + \eta^2/3)^{1/2}\ V_{zz}$, V_{zz} has been converted from atomic units (AU) to mm s^{-1} by using the calibration factor –1.232 mm s^{-1}/AU for Fe^{2+}, which corresponds to a nuclear quadrupole moment Q(^{57}Fe) of 0.123 barn, and –1.478 mm s^{-1}/AU for Fe^{3+}, which corresponds to a nuclear quadrupole moment Q(^{57}Fe) of 0.148 barn. [f] No sign is given in cases where the sign has not been reported. For those cases, the sign of the experimental value has been assumed to be the sign obtained by DFT in the graphs of Figures S6 and S7 from which the calibration factor was determined by linear regression. [g] This system does not shown 2nd order Doppler shift and has been excluded from the calibration analysis.

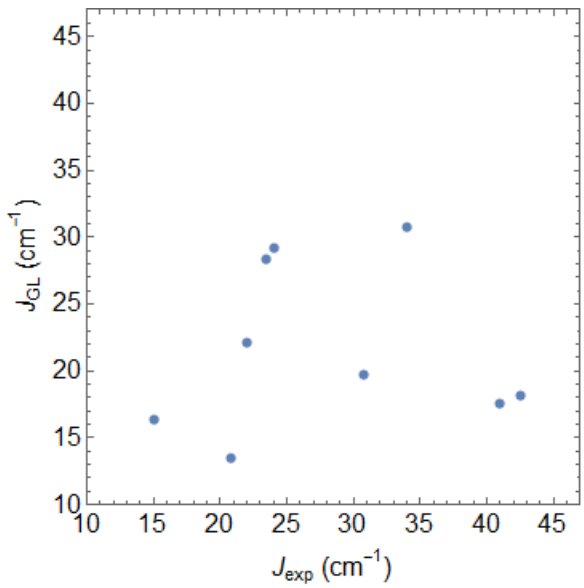

Figure S2. Gorun-Lippard correlation for diferric complexes with hydroxo and alkoxo bridges. J_{GL} vs. J_{exp} (horizontal axis).

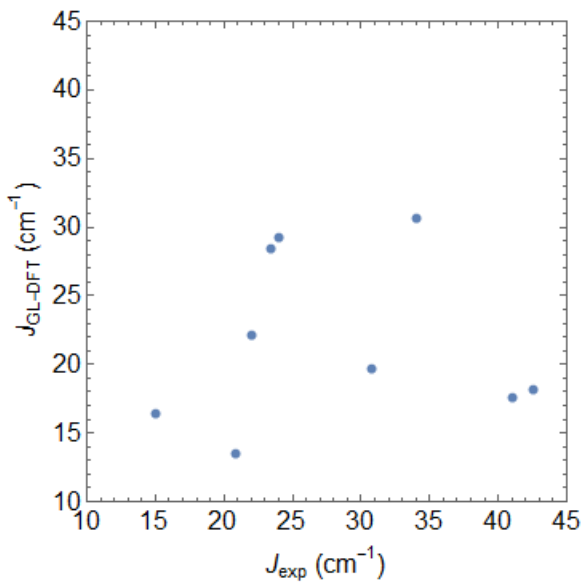

Figure S3. Gorun-Lippard correlation for diferric complexes with hydroxo and alkoxo bridges using DFT distances. J_{GL} vs J_{exp} .

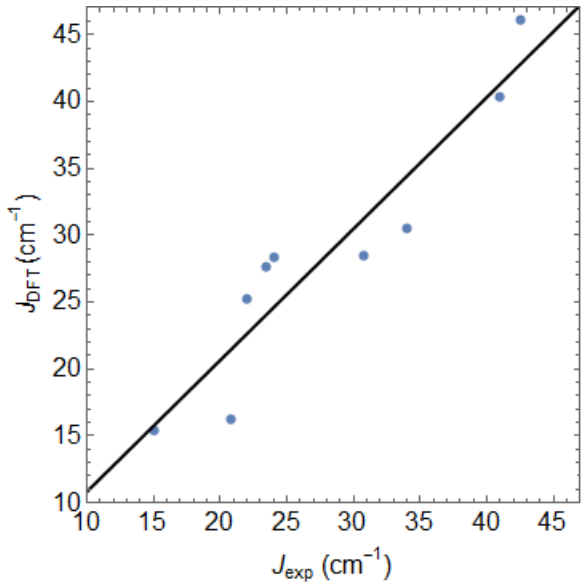

Figure S4. J_{DFT} vs. J_{exp} for diferric complexes with hydroxo and alkoxo bridges (complexes of Tables S4 and S5, excluding PICAFE).

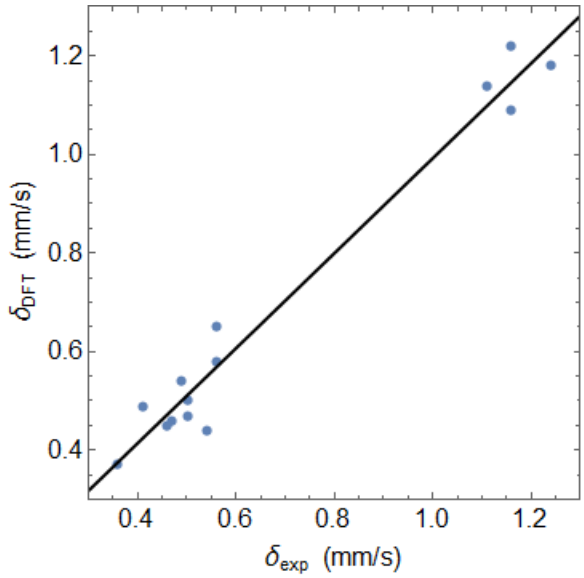

Figure S5. δ_{DFT} vs. δ_{exp} for ferric and ferrous complexes with high-spin iron sites. Average error 0.045 mm/s.

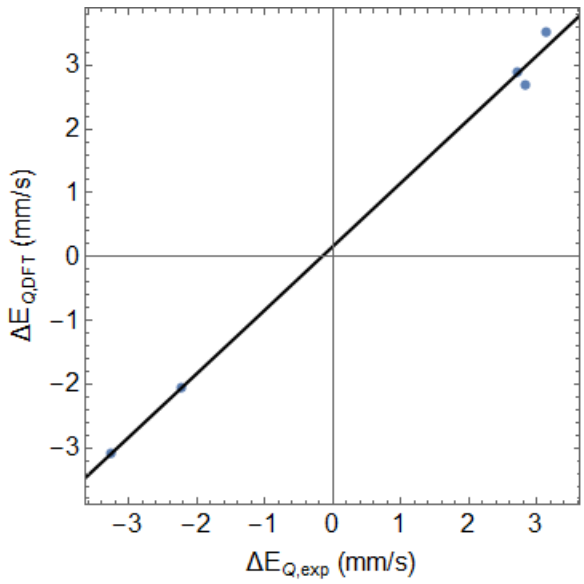

Figure S6. ΔE_Q from DFT vs. ΔE_Q from Mössbauer for ferrous high-spin complexes of Table S2. Average error 0.2 mm/s.

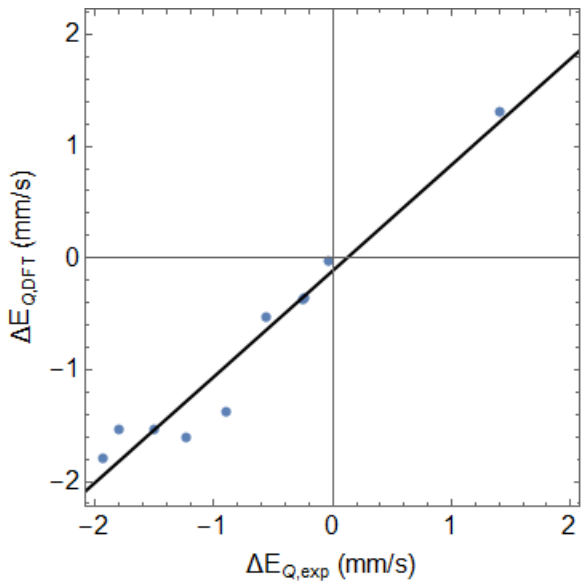

Figure S7. ΔE_Q from DFT vs. ΔE_Q from Mössbauer for ferric high-spin complexes of Table S2. Average error 0.2 mm/s.

Table S7. Comparison of DFT results for J, δ, and ΔE_Q with experiment for diiron(II) model complexes.

CCSD	Bridges	J_{exp} cm^{-1}	J_{DFT} cm^{-1}	δ_{exp} mm/s	δ_{DFT} [c] mm/s	$\Delta E_{Q,exp}$ mm/s	$\Delta E_{Q,DFT}$ [d] mm/s	Ref.[e]
DIBWUG10 [a]	OH, CB, CB	+26	+28	1.16[f,g]	1.21	2.83[k]	+2.68	1
KEZVOA	OR, CB	+22	+22	1.07[f,g]	1.08	+3.13	+2.79	2
XAXRIY [b]	OH, OH_2	+19	+18	1.33[f,h]	1.06/1.05	2.42/2.65[i,j]	+2.48/+2.70[j]	3
KASFUF	OR, OR	–14	–4	1.17[f,g]	1.14	–2.06	–2.53	4

[a] Fe-Fe distance was restrained to the crystallographic value in the DFT gas-phase optimization to prevent elongation of this distance. [b] The atoms of the Fe-water-Fe unit were frozen to their positions in the X-ray structure in the DFT gas-phase optimization to prevent the bridging water from migrating to a terminal position at one the irons. [c] Obtained from DFT using calibration of δ discussed above for ground state. [d] Obtained from DFT using calibration of ΔE_Q presented above. [e] 1, *J. Am. Chem. Soc*. **1987**, *109*, 7387-7396; 2, *J. Am. Chem. Soc*. **1990**, *112*, 6423-6425; 3, *Inorg. Chem*. **2005**, *44*, 8656-8658; *Inorg. Chem*. **1994**, *33*, 2848-2856. [f] Relative to metallic iron at room temperature. [g] Sample temperature is 4.2 K. [h] Sample temperature is 77.9 K. The large difference between δ_{exp} and δ_{DFT} may be due to the constraints in geometry optimization for this system. [i] Values for the two inequivalent iron sites of the complex. [j] Sign of ΔE_Q was not reported.

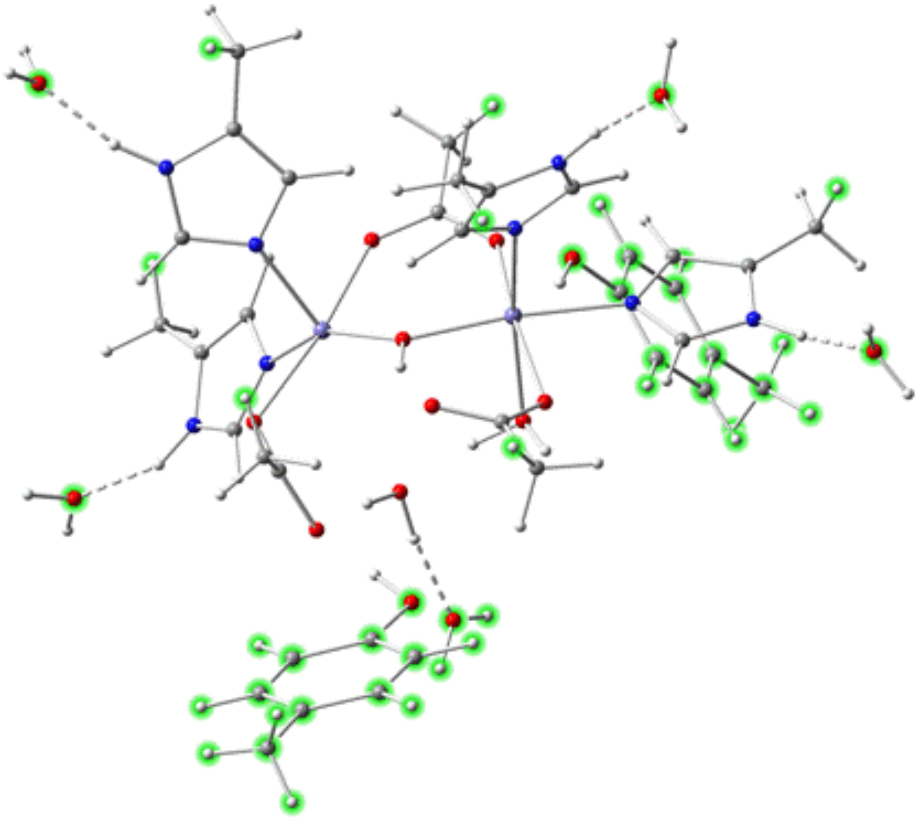

Figure S8. Fixed atoms of optimization are highlighted with green.

Table S8. Mössbauer parameters determined from the zero-field spectra of FDP_{red} recorded at the indicated temperatures.

T (K)	δ (mm/s)	ΔE_Q (mm/s)
4.2	1.16	2.42
25	1.16	2.41
50	1.15	2.40
100	1.14	2.35
150	1.12	2.28

Reference to Gaussian 09:

Revision A.02, M. J. Frisch, G. W. Trucks, H. B. Schlegel, G. E. Scuseria, M. A. Robb, J. R. Cheeseman, G. Scalmani, V. Barone, B. Mennucci, G. A. Petersson, H. Nakatsuji, M. Caricato, X. Li, H. P. Hratchian, A. F. Izmaylov, J. Bloino, G. Zheng, J. L. Sonnenberg, M. Hada, M. Ehara, K. Toyota, R. Fukuda, J. Hasegawa, M. Ishida, T. Nakajima, Y. Honda, O. Kitao, H. Nakai, T. Vreven, J. A. Montgomery, Jr., J. E. Peralta, F. Ogliaro, M. Bearpark, J. J. Heyd, E. Brothers, K. N. Kudin, V. N. Staroverov, R. Kobayashi, J. Normand, K. Raghavachari, A. Rendell, J. C. Burant, S. S. Iyengar, J. Tomasi, M. Cossi, N. Rega, J. M. Millam, M. Klene, J. E. Knox, J. B. Cross, V. Bakken, C. Adamo, J. Jaramillo, R. Gomperts, R. E. Stratmann, O. Yazyev, A. J. Austin, R. Cammi, C. Pomelli, J. W. Ochterski, R. L. Martin, K. Morokuma, V. G. Zakrzewski, G. A. Voth, P. Salvador, J. J. Dannenberg, S. Dapprich, A. D. Daniels, O. Farkas, J. B. Foresman, J. V. Ortiz, J. Cioslowski, and D. J. Fox, Gaussian, Inc., Wallingford CT, 2009.